Deactivation of poly(o-aminophenol) film electrodes by storage without use in the supporting electrolyte solution and its comparison with other deactivation processes. A study employing EIS

R. I. Tucceri

Journal of Applied Electrochemistry

ISSN 0021-891X

J Appl Electrochem
DOI 10.1007/s10800-015-0851-y

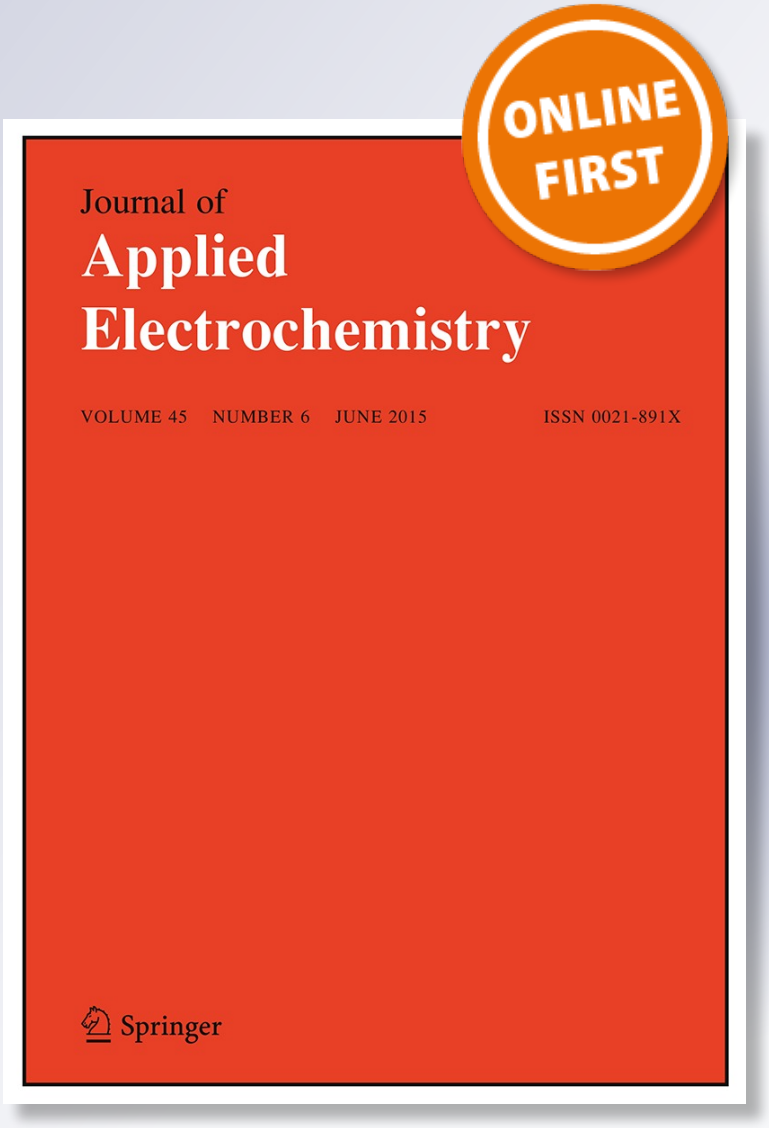

Springer

J Appl Electrochem
DOI 10.1007/s10800-015-0851-y

RESEARCH ARTICLE

Deactivation of poly(*o*-aminophenol) film electrodes by storage without use in the supporting electrolyte solution and its comparison with other deactivation processes. A study employing EIS

R. I. Tucceri[1]

Received: 7 March 2015 / Accepted: 18 May 2015

Abstract The effect of storage time without use (STWU) in the supporting electrolyte solution on the charge-transport parameters of poly(*o*-aminophenol) (POAP) film electrodes was studied by electrochemical impedance spectroscopy. STWU decreases the charge-transport rate of the polymer. This effect is herein called deactivation. Impedance diagrams of both nondeactivated and deactivated films in contact with a solution containing the *p*-benzoquinone/hydroquinone redox couple were interpreted on the basis of a model formulated for homogeneous conducting polymers, where the bathing electrolyte contains a redox pair that provides the possibility for electrons to leak from the film surface. Dependences of diffusion coefficients for electron (D_e) and ion (D_i) transport and interfacial resistances related to ion $\left(R_i^{f|s}\right)$ and electron $\left(R_{m|f}, R_e^{f|s}\right)$ transfer across the polymer/solution and metal/polymer interfaces, respectively, on the degree of deactivation (θ_d) of the polymer were obtained. These dependences were compared with those from previous work for POAP films deactivated by employing other procedures, such as high positive potential limits, soaking in a ferric ion solution, and prolonged potential cycling.

Keywords Poly(*o*-aminophenol) · Deactivation · Storage time · Electrochemical impedance spectroscopy · Charge-transport parameters

✉ R. I. Tucceri
rtucce@gmail.com

[1] Instituto de Investigaciones Fisicoquímicas Teóricas y Aplicadas (INIFTA), CONICET, Facultad de Ciencias Exactas, Universidad Nacional de La Plata, Sucursal 4, Casilla de Correo 16, 1900 La Plata, Argentina

1 Introduction

The oxidation of *o*-aminophenol on different electrode materials (gold, platinum, carbon, indium-tin oxide, etc.) in aqueous acid medium was shown to form poly-*o*-aminophenol (POAP) [1–3]. POAP exhibits its maximal electroactivity within the potential range $-0.2\ \text{V} < E < 0.5\ \text{V}$ (vs. SCE) at pH values lower than 3. The electroactivity of POAP was explained by a redox mechanism that involves an addition/elimination of protons coupled with a reversible electron transfer [4, 5]. Poly(*o*-aminophenol) synthesized in acidic medium is found to be a useful material to build electrochemical sensors and electrocatalysts [6–9]. Also, the copolymer of aniline and *o*-aminophenol poly(aniline-co–*o*-aminophenol)has been synthesized [10] and applied for different purposes, e.g., to develop an electrically controlled anion exchange process to remove perchlorate from industrial wastewaters [11, 12] and for electrocatalytic oxidation and reduction [13, 14]. Considering the interesting applications of POAP, where the polymer is subjected to rugged conditions (prolonged potential cycling (PPC), potential range, storage conditions, etc.) that could cause a decay in electrochemical activity, not many efforts have been made to study POAP deactivation. We have demonstrated that the different electrochemical and chemical treatments PPC [15], high positive potential limits (HPPL) [16], soaking in a ferric ion solution (SFeIS) [17, 18], and storage time without use (STWU) [19]), in which POAP films are subjected to both applied and basic studies, decrease the charge-transport rate of the polymer, affecting its conductivity. This effect is herein called deactivation. The loss of conductivity of an electroactive polymer film is often a problem in electrochemical measurements where the polymer acts as an electron-transfer mediator [16–19]. Very low conduction and permeation are, for instance, observed in passivating polymeric films deposited on

Published online: 30 May 2015

electrode surfaces [20]. In this regard, during the electrochemical analysis or disposal of most phenolic compounds, insulated polymeric substrates are created and cover the electrode surface. This can cause the signal current to decay over time, which is called electrode fouling or electrode passivation [20].

With regard to POAP deactivation, it was recently demonstrated that STWU in the supporting electrolyte solution for time periods longer than 32 h strongly reduces the polymer electroactivity. The effect of STWU on the electron transport rate of POAP film electrodes was studied in previous work employing cyclic voltammetry, rotating disk electrode voltammetry (RDEV), and surface resistance (SR) [19]. This deactivation is evidenced by an attenuation of the voltammetric response, which allows one to define a degree of deactivation (θ_d). RDEV experiments carried out in [19] with both deactivated and nondeactivated films in the presence of the hydroquinone/*p*-benzoquinone (HQ/Q) redox couple were interpreted in terms of the electron hopping model. A decrease of the electron transport rate (D_e) with the increase in the degree of deactivation of POAP films was observed. This effect was explained on the basis of an increase in the electron hopping distance between two adjacent redox sites as the degree of deactivation increases. A higher distance between adjacent redox sites in a deactivated POAP film than in a nondeactivated one is consistent with SR results, where the more deactivated the film is, the more diffuse the reflection of the conduction electrons of gold at the gold film/POAP film interface becomes. In order to obtain a more complete series of charge-transport parameters than those obtained from RDEV measurements [19], electrochemical impedance spectroscopy (EIS) measurements were carried out in the present work. Impedance diagrams of POAP films, in the presence of the same redox couple employed in [19], were interpreted on the basis of a model formulated by Vorotyntsev et al. [21]. Charge-transport parameters obtained in this work for POAP films deactivated by STWU are compared with those obtained in other studies for POAP films deactivated employing other procedures such as PPC [15], HPPL [16], and SFeIS [17, 18]. It should be remarked that in the present work, as in previous ones [15–19], we are only interested in analyzing the effects of different electrochemical and chemical treatments on the charge propagation process of POAP films. That is, it is expected that after reading this paper, researchers will pay attention to the limits of stability and durability of POAP, particularly with regard to maintenance of its conducting properties under different chemical and electrochemical treatments. It is not the aim of the present work to differentiate the physicochemical phenomena involved in POAP deactivation employing different treatments. In this regard, further work is in progress to elucidate the chemical and physical transformations that alter the conducting properties of a POAP film after being subjected to different treatments such as PPC, HPPL, SFeIS, and STWU.

2 Experimental

The same gold rotating disk electrode (RDE) described in [19] was used as base electrode to deposit POAP films. Also, POAP films were synthesized from a 10^{-3} M *ortho*aminophenol + 0.4 M $NaClO_4$ + 0.1 M $HClO_4$ solution and stabilized in the supporting electrolyte (0.4 M $NaClO_4$ + 0.1 M $HClO_4$) solution, as previously described [19]. These POAP films are herein called nondeactivated films. These films were deactivated employing the same procedure described in [19]. That is, the same series of eight POAP-coated RDEs listed in Table 1 of Ref. [19] was prepared in this work, and each one of them was successively deactivated in the supporting electrolyte solution employing the same storage time sequence listed in Table 1 of Ref. [19]. A degree of deactivation (θ_d) was also defined here on the basis of the attenuation of the voltammetric response by employing Eq. (1) [19] as

$$\theta_d = 1 - \left(Q_{Red,c}/Q_{Red,T}\right), \quad (1)$$

where $Q_{Red,c}$ is the total reduction charge assessed by integration of the corresponding voltammetric response for a deactivated film, and $Q_{Red,T} = 2.8$ mC cm^{-2} is the total reduction charge for the nondeactivated film. Thus, for a nondeactivated POAP film, the degree of deactivation was $\theta_d = 0$, taking $Q_{Red,T} = 2.8$ mC cm^{-2} as reference charge. However, values of $\theta_d > 0$ are indicative of POAP films that have been deactivated by storage in the supporting electrolyte solution. Then, with both nondeactivated and deactivated POAP films, RDEV experiments were performed in the presence of a solution containing equimolar concentrations of *p*-benzoquinone (Q) and hydroquinone (HQ) species (0.1 M $HClO_4$ + 0.4 M $NaClO_4$ + 2 × 10^{-3} M Q/HQ). Impedance spectra of deactivated and nondeactivated POAP films in contact with the redox couple were measured following a 30-min application of the steady-state potential in the range from −0.2 V to 0.0 V (SCE). Impedance values for different degrees of deactivation (θ_d) were determined at seven discrete frequencies per decade with a signal amplitude of 5 mV. Impedance spectra were validated by Kramers–Kronig transformations. Impedance diagrams at potential values corresponding to the reduced state of POAP were only considered in this work because the impedance model described in [21] was developed within the framework of the assumption that the redox active species (HQ/Q) are only present in the solution phase but not inside the film, and they participate in the interfacial electron exchange within the polymer at the film/solution boundary. At

potential values more positive than 0.4 V (SCE), the redox couple is incorporated into the POAP film.

A large-area gold grid was used as counter electrode. All the potentials are referred to the SCE. Impedance measurements in the frequency range 0.01 Hz–10 kHz were performed with a PAR 309 system.

3 Results and discussion

3.1 Different charge-transport and charge-transfer parameters of POAP films deactivated by storage and their dependence on the degree of deactivation

Impedance diagrams of nondeactivated and deactivated POAP films are shown in Figs. 1, 2, 3. Solid lines are simulated curves calculated by Eq. (2) [21] (see Appendix). As it is often considered that some transformed curves could give more valuable information about the goodness of the fitting than Nyquist plots, real and imaginary parts versus frequency plots corresponding to each one of the Nyquist representations were also built. One of these representations for a θ_d value of 0.41 is shown in Fig. 4. Although several *ac* impedance diagrams at potential values within the range −0.2 V to 0.0 V (SCE) were recorded for different POAP films, those shown in Figs. 1 2, 3, 4 were considered as representative of the potential region where POAP is in its reduced state. A good fitting was observed for the different impedance diagrams. The fitting procedure using Eq. (2) was based on the complex nonlinear squares (CNLS) method (see Appendix).

In the simulations, the number of transferred electrons, n, reported in [22] was employed, and diffusion coefficient values of the redox species (Q and HQ) were considered

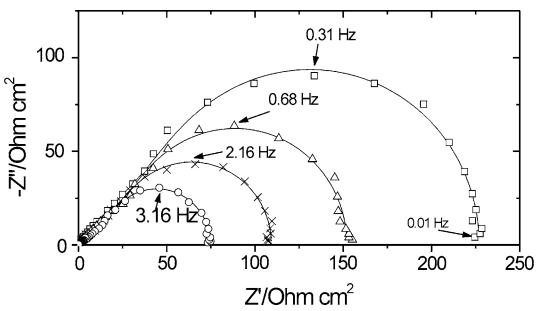

Fig. 1 *Ac* impedance diagrams in the Nyquist coordinates ($-Z''$ vs. Z) obtained at $E = -0.2$ V for a nondeactivated POAP film. The different diagrams correspond to different electrode rotation rates, Ω: (*open rectangle*) 100 rpm; (*open triangle*) 200 rpm; (*multiplication*) 300 rpm; (*open circle*) 600 rpm. Electrolyte: 0.1 M $HClO_4$ + 0.4 M $NaClO_4$ + 2 × 10^{-3} M (HQ/Q) solution. Discrete points are experimental data, and *solid lines* represent the fitting using the theory described in [21]

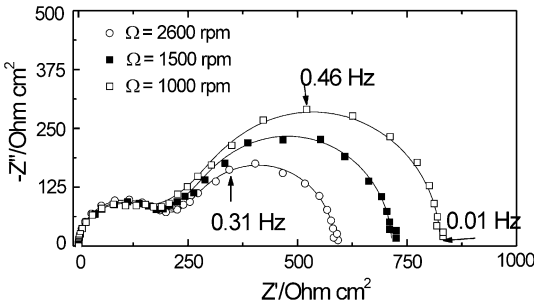

Fig. 2 *Ac* impedance diagrams in the Nyquist coordinates ($-Z''$ vs. Z) obtained at $E = -0.2$ V for a deactivated POAP film, $\theta_d = 0.62$. The different diagrams correspond to different electrode rotation rates, Ω, indicated in the figure. Electrolyte: 0.1 M $HClO_4$ + 0.4 M $NaClO_4$ + 2 × 10^{-3} M (HQ/Q) solution. Discrete points are experimental data, and *solid lines* represent the fitting using the theory given in [21]

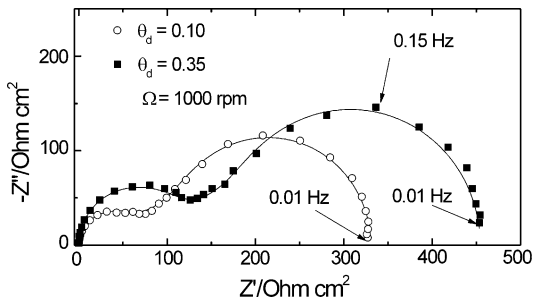

Fig. 3 *Ac* Impedance diagrams in the Nyquist coordinates ($-Z''$ vs. Z) obtained at $E = -0.2$ V and a constant electrode rotation rate, $\Omega = 1000$ rpm, for two deactivated POAP films: (*open circle*) $\theta_d = 0.10$; (*open rectangle*) $\theta_d = 0.35$. Electrolyte: 0.1 M $HClO_4$ + 0.4 M $NaClO_4$ + 2 × 10^{-3} M (HQ/Q) solution. Discrete points are experimental data, and *solid lines* represent the fitting using the theory given in [21]

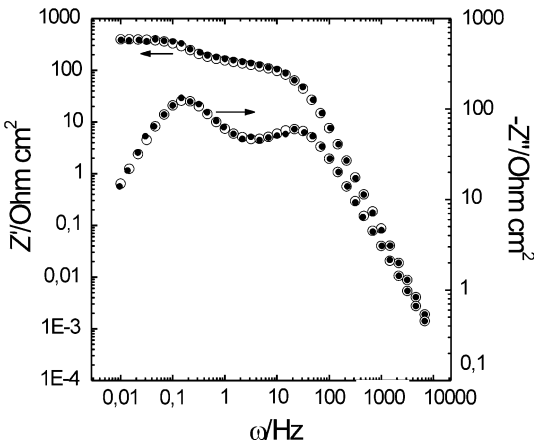

Fig. 4 Real part (Z') and imaginary part ($-Z''$) versus frequency (ω) plots (point-to-point representations) for a POAP film with $\theta_d = 0.41$. $E = -0.2$ V, $\Omega = 3000$ rpm. Electrolyte: 0.1 M $HClO_4$ + 0.4 M $NaClO_4$ + 2 × 10^{-3} M (HQ/Q) solution. (*open circle*) Experimental data; (*bullet*) fitting using Eq. (1) [21]

equal, $D_{ox,red} = 1.5 \times 10^{-5}$ cm^2 s^{-1}. Also, the bulk concentrations of the redox substrate species were considered equal ($c_{ox} = c_{red} = 2 \times 10^{-6}$ mol cm^{-3}). The polymer thickness was $\phi_p = 60$ nm [19]. The value of the total redox site concentration of POAP was $c_o = 4.7 \times 10^{-3}$ mol cm^{-3} [1]. The ohmic resistance of the solution in contact with the polymer films, R_S, was measured. A value $R_S \sim 2.14$ ohm cm^2 was obtained. Then, by considering the high-frequency intercept of impedance diagrams of POAP films in the presence and in the absence of the redox couple in solution as R_o, the high-frequency bulk POAP film resistance, R_f, was calculated as $R_f = R_o - R_S$ [23]. The latter value varied within the range $1.27 < R_f < 2.01$ ohm cm^2 and it seems not to be strongly dependent on the degree of deactivation. Then, R_f and R_S values were imposed on the fitting. The other parameters contained in Eq. (2) $\left(R_{m|f}, R_i^{f|s}, R_{m|f}, R_i^{f|s}, R_e^{f|s}, C_p, D_e \text{ and } D_i\right)$ were calculated from the experimental impedance data by the fitting procedure described above. The first three parameters $\left(R_{m|f}, R_i^{f|s} \text{and } R_e^{f|s}\right)$ were varied without restraints during the fitting. However, some reference values were considered for C_p, D_e, and D_i. For the nondeactivated POAP film thickness used in this work ($\phi_p = 60$ nm) and solution pH 1, D_e and D_i values were allowed to vary within the range 10^{-7}–10^{-11} cm^2 s^{-1}, in such a way that diffusion coefficient values lower than 10^{-11} were considered unrealistic for these thick films. That is, D_e and D_i values lower than 10^{-11} were only obtained from impedance diagrams (not shown) of very thin POAP films $(Q_{T,Red} = 0.2\,\text{mC cm}^{-2}, \phi_p = 10\,\text{nm})$ contacting solutions of pH 1, where incomplete coating of the metal area by the thin polymer film is possible. Concerning C_p, reference values were extracted from experimental $-Z''$ versus ω^{-1} slopes of impedance diagrams at sufficiently low frequency (in the absence of the redox substrate in solution). A contribution of the interfacial capacitance, C_H, also considered as a fitting parameter, was included in order to represent the actual impedance diagrams from the calculated ones.

Different charge-transport and charge-transfer parameters versus θ_d dependences for a POAP film deactivated by STWU, extracted from the fitting procedure described above, are shown from Figs. 5, 6, 7, 8, 9, 10.

The C_p versus θ_d dependence is shown in Fig. 5. As can be seen, starting from a C_p value of about 27 F cm^{-3}, for a nondeactivated film, a decrease of C_p with increasing θ_d is observed. This decrease is consistent with the continuous attenuation of the voltammetric response as the degree of deactivation increases [19]. It should be kept in mind that these C_p values correspond to the reduced state of POAP. There was no difference in the redox capacitance versus θ_d dependence achieved in the supporting electrolyte from the

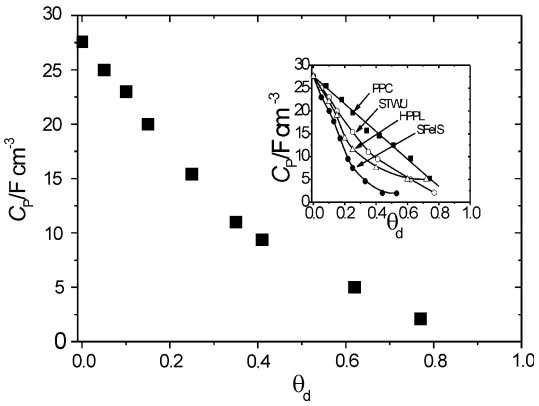

Fig. 5 Redox capacitance (C_p) as a function of θ_d for a POAP film deactivated by STWU. The value 27.5 F cm^{-3} for $\theta_d = 0$ corresponds to a nondeactivated film. Electrolyte: 0.1 M $HClO_4$ + 0.4 M $NaClO_4$ + 2×10^{-3} M (HQ/Q) solution. *Inset* C_p as a function of θ_d for the different deactivation processes

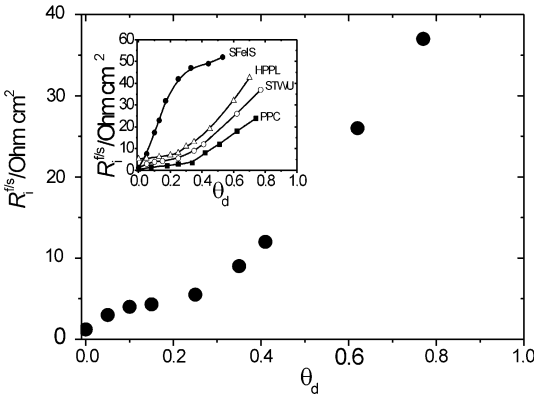

Fig. 6 Polymer–solution interfacial ion-transfer resistance $\left(R_i^{f/s}\right)$ as a function of θ_d for a POAP film deactivated by STWU. Electrolyte: 0.1 M $HClO_4$ + 0.4 M $NaClO_4$ + 2×110^{-3} M (HQ/Q) solution. *Inset* $R_i^{f/s}$ as a function of θ_d for the different deactivation processes

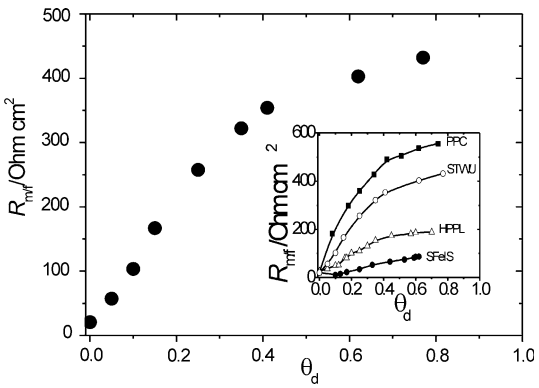

Fig. 7 Metal–polymer interfacial electron-transfer resistance ($R_{m/f}$) as a function of θ_d for a POAP film deactivated by STWU. Electrolyte: 0.1 M $HClO_4$ + 0.4 M $NaClO_4$ + 2×110^{-3} M (HQ/Q) solution. *Inset* $R_{m/f}$ as a function of θ_d for the different deactivation processes

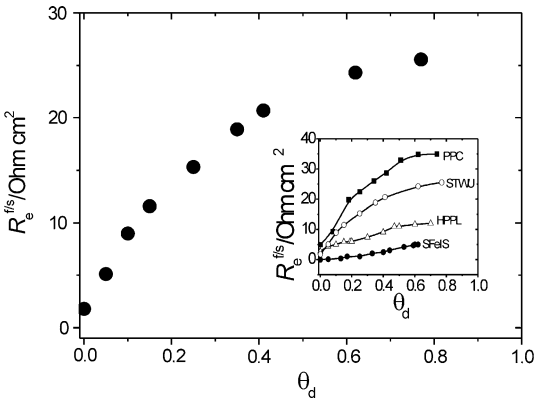

Fig. 8 Interfacial electron-transfer resistance $\left(R_e^{f/s}\right)$ as a function of θ_d for a POAP film deactivated by STWU. Electrolyte: 0.1 M $HClO_4$ + 0.4 M $NaClO_4$ + 2 × 10^{-3} M (HQ/Q) solution. *Inset* $R_e^{f/s}$ as a function of θ_d for the different deactivation processes

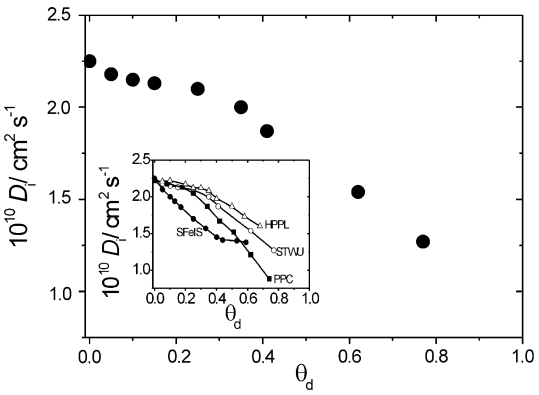

Fig. 9 Ion diffusion coefficient (D_i) as a function of θ_d for a POAP film deactivated by STWU. Electrolyte: 0.1 M $HClO_4$ + 0.4 M $NaClO_4$ + 2 × 10^{-3} M (HQ/Q) solution. *Inset* D_i as a function of θ_d for the different deactivation processes

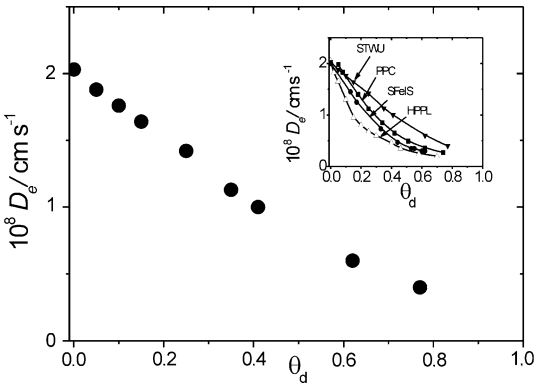

Fig. 10 Electron diffusion coefficient (D_e) as a function of θ_d for a POAP film deactivated by STWU. Electrolyte: 0.1 M $HClO_4$ + 0.4 - M $NaClO_4$ + 2 × 10^{-3} M (HQ/Q) solution. *Inset* D_e versus θ_d dependence for different deactivation processes

$-Z''$ versus ω^{-1} slopes and in the presence of the redox active substrate from Eq. (2). Only small differences in the numerical values of C_p were found. The good agreement between the redox capacitance values attained under these different conditions could be considered as an indication of the high fitting accuracy reached to obtain optimum parameter values (in this case C_p) for the treated system using Eq. (2).

The dependences of $R_i^{f|s}$ and R_{mlf} on θ_d are shown in Figs. 6 and 7, respectively. $R_i^{f|s}$ as a function of θ_d exhibits a different feature than that of R_{mlf}. That is, while R_{mlf} seems to change continuously within the whole θ_d range, $R_i^{f|s}$ firstly exhibits a slight increase within the range $0 < \theta_d < 0.30$ and then, a strong increase within the range $0.35 < \theta_d < 0.77$. Also, the magnitude of the R_{mlf} and $R_i^{f|s}$ change within the whole θ_d range is different. The $R_i^{f|s}$ change is around one order of magnitude lower than the R_{mlf} change. This difference could indicate that the high-frequency semicircle on the impedance diagrams (Figs. 1, 2, 3) is mainly determined by R_{mlf}. The increase of interfacial R_{mlf} resistance could be due to an increasing number of inactive sites at the metal/polymer interface with the increase in the degree of deactivation [19].

$R_e^{f|s}$ values were extracted from Eq. (4) (see Appendix) using k as fitting parameter $(0.01 < k < 1000\,\text{cms}^{-1})$. The characteristic of the $R_e^{f|s}$ versus θ_d dependence (Fig. 8) is similar to that of the $R_{m/f}$ versus θ_d dependence. However, $R_e^{f|s}$ values are around one order of magnitude lower than $R_{m/f}$ values.

Also, it is interesting to note that at a degree of deactivation lower than 0.4, $R_e^{f|s}$ values are higher than $R_i^{f|s}$ values. Then, the storage without use seems to more strongly affect the polymer/solution interfacial electron-transfer resistance, $R_e^{f|s}$, than the polymer/solution interfacial ion-transfer resistance $R_i^{f|s}$. The increase in interfacial $R_e^{f|s}$ resistance could be due to an increasing number of inactive sites at the polymer/solution interface with the increase in the degree of deactivation.

Ion and electron diffusion coefficients versus θ_d dependences are shown in Figs. 9 and 10, respectively. Both diffusion coefficients decrease as θ_d increases. As was proposed from RDEV data [19], the decrease of D_e with the increase of θ_d could be attributed to an increase in the hopping distance between redox active sites after polymer deactivation. D_e values are nearly two orders of magnitude higher than D_i values. It is possible that electron hopping controls the charge-transport process at a POAP film in its oxidized state, where the polymer is swollen, which facilitates ion transport. However, in the present work, relative diffusion coefficient values ($D_e > D_i$) refer to the

reduced state of POAP. As can be seen by comparing Fig. 10 of this paper with Fig. 4 of Ref. [19], the Vorotyntsev's model gives D_e values almost three orders of magnitude higher than the D_e values extracted from RDEV. In this regard, the interpretation of diffusion coefficients at polymer films depends on the model employed to describe the charge propagation and, sometimes, on the technique used in its measurement. Another interesting difference between D_e and D_i versus θ_d dependences can be observed by comparing Fig. 9 with Fig. 10. While D_i is reduced one half in going from θ_d–0 to θ_d–0.77, D_e is reduced approximately four times. This finding would mean that although ion motion always controls the charge-transport process at POAP films, the influence of electron motion on the whole charge-transport process becomes more pronounced at a high degree of deactivation. With regard to D_e and D_i versus θ_d dependences, while a continuous decrease is observed for D_e within the whole θ_d range, a break around $\theta_d \sim 0.30$ seems to be observed in the D_i versus θ_c^d dependence. Such break also becomes evident in the $R_i^{f|s}$ versus θ_d dependence (Fig. 6). Probe beam deflection measurements [24] suggest that while protons and anions are exchanged during POAP oxidation, insertion of protons is the dominant process during the POAP reduction process. Also, impedance measurements reported in [25] indicate that POAP is only doped with hydrogen ions, and the effect of anions is negligible. Then, it is possible that both parameters $R_i^{f|s}$ and D_i are related to proton movements across the POAP/solution interface and inside the polymer film, respectively, rather than to anion transport. Concerning the proton movement into POAP films, the existence of two forms (mobile and bound) of hydrogen ions in the bulk film has been proposed [25]. It was suggested that in polymers derived from aromatic amines, hydrogen ions could be constrained by nitrogen atoms of polymer chains and do not contribute to the electrical conductance of the film, and another part of such constrained groups is able to dissociate producing the mobile form of hydrogen, which provides the film conductance. In other words, besides mobile protons, some traps for hydrogen ions within the bulk of the film may be present, which provides the binding of these protons with polymer film fragments. This proton conduction mechanism is similar to that proposed for ion transport in some solid-state materials [26], where ion movement occurs by a hopping process with the participation of two different types of sites. While some sites allow a fast ion diffusion process, other sites immobilize ions and do not allow them to participate in the diffusion process. The existence of these different types of sites was explained in terms of different energy barriers [26]. In this regard, the slight increase in the $R_i^{f|s}$ versus θ_d (the slight decrease in the D_i vs. θ_d) dependence within the range $0 < \theta_d < 0.30$ could be due to the inhibition of traps for hydrogen ions, which only causes a small ion conductivity change. However, the strong $R_i^{f|s}$ increase (more pronounced D_i decrease) for $\theta_d > 0.35$ could be attributed to the inhibition of nitrogen-containing groups that provide the binding of hydrogen ions and at the same time are able to dissociate and give the mobile form of hydrogen that markedly contributes to the polymer conductivity.

With regard to C_H values, starting from a value of around 17 μF cm^{-2} for a nondeactivated film, C_H decreases in a nearly continuous way as the degree of deactivation increases, reaching a value of about 7.5 μF cm^{-2} for $\theta_d \sim 0.77$ (not shown). The C_H decrease, as well as the R_{mlf} increase, could be assigned to the creation of inactive gaps in the redox site configuration at the polymer/metal interface with deactivation.

3.2 Effect of different deactivation procedures on the charge-transport parameters of POAP films extracted from EIS

Dependences of charge-transport and charge-transfer parameters on the degree of deactivation of POAP films subjected to STWU (this work), PPC [15], HPPL [16], and SFeIS [17, 18] extracted from EIS are compared in this section.

As can be seen by comparing the four D_e versus θ_d dependences shown in the inset of Fig. 10 with those obtained from RDEV data (see inset in Fig. 4 in [19]), although diffusion coefficient values obtained from the Vorotyntsev et al.'s model [21] are three orders of magnitude higher than those obtained from RDEV, the same sequence of D_e values is obtained from both techniques, i.e., at each θ_d value D_e (STWU) > D_e (PPC) > D_e (SFeIS) > D_e (HPPL). The consistence of the electron diffusion coefficient sequences obtained from EIS and RDEV measurements could allow one to interpret again the rate of electron transport extracted from EIS in terms of different redox site distributions according to the deactivation procedure employed. In this regard again, the more spread redox site distribution should correspond to a POAP film deactivated applying HPPL, as compared with the other deactivation procedures.

By comparing the insets in Figs. 7 and 8, it is interesting to note that R_{mlf} and $R_e^{f|s}$ resistances follow the same sequence for the different deactivation processes. That is, while the stronger increase is observed for a POAP films subjected to PPC, the interaction with a ferric ion solution causes the lower effect on the electron transfers across the metal/polymer and polymer/solution interfaces. The effects of STWU and HPPL seem to be intermediate between those caused by

PPC and SFeIS. The sequence followed by R_{mlf} and $R_e^{f|s}$ is different from those followed by the electron diffusion coefficient (inset in Fig. 10) and the potentiodynamic $\Delta R/R$ change (Fig. 10 in [19]). In this connection, it should be kept in mind that while D_e is related to the bulk electron transport, R_{mlf} and $R_e^{f|s}$ are related to interfacial electron transfers. Also, although R_{mlf}, like the potentiodynamic$\Delta R/R$ change, is related to the metal/polymer interface, both R_{mlf} and $\Delta R/R$ resistances cannot be directly related because R_{mlf} is associated with a transversal charge motion due to the electron transfer across the polymer/metal interface, while the $\Delta R/R$ change is attributed to the scattering of conduction electrons from the inside of the metal to the metal/polymer interface caused by changes in the translational symmetry parallel to the interface due to the presence of a different distribution of scatterers (redox sites) at the interface.

As was indicated, $R_i^{f|s}$ and D_i at POAP seem to be related to proton transfer across the polymer/solution interface and proton diffusion across the film, respectively. The sequence followed by the polymer–solution interfacial ion-transfer resistance $R_i^{f|s}$ as a function of θ_d (inset in Fig. 6) for the different deactivation processes is opposite to those followed by R_{mlf} and $R_i^{f|s}$. In this regard, the stronger restriction (higher $R_i^{f|s}$ value) for the proton transfer at the polymer/solution interface seems to be caused by the interaction of ferric ions with POAP. Also, as can be seen from the inset in Fig. 9, although D_i as a function of θ_d for the different deactivation processes does not follow the same sequence as $R_i^{f|s}$ versus θ_d, the incorporation of ferric ions into the POAP matrix causes a more pronounced decrease in the ion diffusion coefficient value than in the other deactivation procedures. Thus, soaking of POAP in a ferric ion solution seems to mainly affect proton diffusion across the film and proton transfer across the POAP/solution interface. In this regard, deactivation of POAP by SFeIS has been attributed to the direct interaction of iron ions with the redox sites of POAP, which impedes the protonation reaction of the polymer [27]. The redox capacitance (inset in Fig. 5) seems to be strongly affected by the incorporation of iron ions into the POAP matrix. PPC affects this impedance value to a lesser extent. STWU and HPPL seem to cause intermediate effects on the redox capacitance. The same characteristics are observed in $R_i^{f|s}$ versus θ_d dependence (inset in Fig. 6).

4 Conclusions

While diffusion coefficients for electron (D_e) and ion (D_i) transport decrease, interfacial resistances related to ion ($R_i^{f|s}$) and electron $\left(R_{m|f}, R_e^{f|s}\right)$ transfer across the polymer/solution and metal/polymer interfaces, respectively, increase with the degree of deactivation of a POAP film subjected to STWU. A decrease of the redox capacitance with the increase in the degree of deactivation is also observed for a POAP film deactivated by STWU. These dependences were compared with those obtained from POAP films subjected to other deactivation procedures such as PPC, SFeIS, and HPPL. At constant degree of deactivation, the electron transport rate follows the order D_e (STWU) > D_e (PPC) > D_e (SFeIS) > D_e (HPPL), i.e., the greatest effect on the electron transport was observed for a POAP film deactivated by HPPL. R_{mlf} and $R_e^{f|s}$ resistances follow the same sequence for the different deactivation processes. That is, while the strongest increase is observed for a POAP films subjected to PPC, the interaction with a ferric ion solution causes the smallest effect on the electron transfers across the metal/polymer and polymer/solution interfaces.

$R_i^{f|s}$ and D_i at POAP were related to proton transfer across the polymer/solution interface and proton diffusion across the film, respectively. $R_i^{f|s}$, as a function of the degree of deactivation for the different deactivation processes, is opposite to those followed by R_{mlf} and $R_e^{f|s}$. In this regard, the strongest restriction (higher $R_i^{f|s}$ value) for the proton transfer at the polymer/solution interface seems to be caused by the interaction of ferric ions with POAP. Although D_i, as a function of the degree of deactivation for the different deactivation processes, does not follow the same sequence as $R_i^{f|s}$ does, the incorporation of ferric ions into the POAP matrix causes the most pronounced decrease in the ion diffusion coefficient value as compared with the other deactivation procedures. Thus, soaking of POAP in a ferric ion solution seems to mainly affect the proton diffusion across the film and the proton transfer across the POAP/solution interface. The redox capacitance is also strongly affected by the incorporation of iron ions into the POAP matrix. PPC affects this impedance value to a lesser extent.

Acknowledgments The author gratefully acknowledges the ConsejoNacional de InvestigacionesCientíficas y Técnicas (CONICET) and also the Facultad de Ciencias Exactas, National University of La Plata (UNLP).

Conflict of interest The authors declare that they have no conflict of interest.

Appendix: interpretation of ac impedance diagrams

A particular interpretation of impedance data is based on the choice of a certain equivalent electrical circuit as a model for the system under study or by introducing a

number of additional elements corresponding to peculiar features of the impedance spectra into the available circuits. However, a correct microscopic formulation of the problem of a modified electrode impedance and its solution for homogeneous conducting polymer films has been reported by Vorotyntsev in [28] and then, extended to the case where the bathing electrolyte contains a redox pair that provides the possibility for the electron to leak from the film surface [21, 29]. The general theory of Vorotyntsev et al. considers diffusion-migration transport of electrons and ions as mobile charge carriers in a uniform medium, coupled with a possibly nonequilibrium charge transfer across the corresponding interfaces at the boundary of the film [30]. "Essentially, the approach is based on the formulae of the multicomponent diffusion" [31] relating the electrochemical potential gradients of flux components. Standard Nernst–Planck–Einstein expressions are used for flux densities of both species (electrons and ions) taking account of both diffusion and migration transport mechanisms. On the basis of the experimental arrangement used in this work, i.e., a gold disk electrode of low surface roughness (high specularity) after deposition by evaporation of a thin gold film coated with a thick POAP film [19], the system could be considered as a good enough approximation to a uniform polymer layer deposited on a smooth electrode surface to apply a homogeneous electrochemical impedance model in the interpretation of experimental *ac* impedance diagrams. Then, the microscopic formulation of *ac* impedance of a modified electrode described by Vorotyntsev et al. in [21] was employed in this work to interpret impedance data of nondeactivated and deactivated POAP films. It should be remarked that the theory developed in [21] is strictly valid when the charging of interfacial double layers is negligible, i.e., it does not account for the charging of the film/substrate and film/solution layers in parallel with the injection processes of charge carriers. If this is not the case, a more complete model, such as the one developed by Vorotyntsev in [28], should be used. In this model [28], besides the traditional "double-layer" capacitance and interfacial charge-transfer resistances, two additional parameters for each boundary, "interfacial numbers" for each species and "asymmetry factors," are introduced. Although we also fitted our experimental impedance diagrams with the model reported in [28], the fitting did not result much more precise than that using the model given in [21], and furthermore, the increasing mathematical difficulty of determining the numerous parameters of the model given in [28] from experimental data was a major drawback. Then, despite this last theoretical limitation, the model described in [21] concerning a uniform and nonporous film and no penetration of redox species from the solution was employed to interpret our experimental impedance diagrams.

As in the present case, one has the modified electrode geometry with a redox active electrolyte solution (m/film/es), Eq. (2) [21] must be applied.

$$Z_{\mathrm{m|film|es}} = R_{\mathrm{m|f}} + R_{\mathrm{f}} + R_{\mathrm{s}} + \left[Z_{\mathrm{e}}^{\mathrm{f|s}} R_{\mathrm{i}}^{\mathrm{f|s}} + W_{\mathrm{f}} Z_{12}^{\mathrm{m}}\right]\left(Z_{\mathrm{e}}^{f|s} + R_{i}^{f|s} + 2W_{\mathrm{f}} \coth 2v\right)^{-1}, \tag{2}$$

where

$$Z_{12}^{\mathrm{m}} = Z_{\mathrm{e}}^{\mathrm{f|s}}\left[\coth v + (t_{\mathrm{e}} - t_{\mathrm{i}})^2 \tanh v\right] + R_{\mathrm{i}}^{\mathrm{f|s}} 4t_{\mathrm{i}}^2 \tanh v + W_{\mathrm{f}} 4t_{\mathrm{i}}^2. \tag{3}$$

In Eqs. (2) and (3), $v = \left[\left(j\omega\phi_{\mathrm{p}}^2\right)\Big/4D\right]^{1/2}$ is a dimensionless function of the frequency ω, ϕ_{p} is the film thickness, D is the binary electron–ion diffusion coefficient, and t_{i} and t_{e} are the migration (high frequency) bulk-film transference numbers for anions and electrons, respectively. D is defined as $D = 2D_{\mathrm{i}}\ D_{\mathrm{e}}\ (D_{\mathrm{e}} + D_{\mathrm{i}})^{-1}$ and $t_{\mathrm{i,e}} = D_{\mathrm{i,e}}\ (D_{\mathrm{e}} + D_{\mathrm{i}})^{-1}$, where D_{e} and D_{i} are the diffusion coefficients for the electrons and ion species, respectively.

$W_{\mathrm{f}} = \left[v/j\omega\phi_{\mathrm{p}}C_{\mathrm{p}}\right] = \Delta R_{\mathrm{f}}/v$ is a Warburg impedance for the electron–ion transport inside the polymer film. $\Delta R_{\mathrm{f}}\left(= \phi_{\mathrm{p}}/4DC_{\mathrm{p}}\right)$ is the amplitude of the Warburg impedance inside the film, and C_{p} is the redox capacitance per unit volume.

R_{f} (= ϕ_{p}/κ) is the high-frequency bulk-film resistance, R_{s} is the ohmic resistance of the bulk solution (κ is the high-frequency bulk conductivity of the film), R_{mlf} is the metal/film interfacial electron-transfer resistance, and $R_{\mathrm{i}}^{\mathrm{f|s}}$ is the film/solution interfacial ion-transfer resistance.

$Z_{\mathrm{e}}^{\mathrm{f|s}} = \left(R_{\mathrm{e}}^{\mathrm{f|s}} + W_{\mathrm{s}}\right)$ is the electronic impedance, where $R_{\mathrm{e}}^{\mathrm{f|s}}$ is the interfacial electron-transfer resistance at the film/solution interface, and W_{s} is the convective diffusion impedance of redox species in solution, which contains the bulk concentrations of ox(red) forms, $c_{\mathrm{ox}}(c_{\mathrm{red}})$, and their diffusion coefficients inside the solution, $D_{\mathrm{ox}}(D_{\mathrm{red}})$. Also, it contains the Nernst layer thickness, δ.

$R_{\mathrm{e}}^{\mathrm{f|s}}$ is defined as

$$R_{\mathrm{e}}^{\mathrm{f|s}} = RT\left(nF^2 k\, c_{\mathrm{red}}\right)^{-1}, \tag{4}$$

where k is the rate constant of the reaction between the film and the redox active forms in solution. The diffusion of the redox forms from the bulk solution to the film/solution interface can be regarded as stationary through the diffusion layer thickness, expressed in cm by

$$\delta = 4.98 D_{\mathrm{ox,red}}^{1/3} \eta^{1/6} \Omega^{-1/2}, \tag{5}$$

where η is the kinematic viscosity of the solution in the same units as $D_{ox,red}$, and Ω the rotation rate of the disk electrode in rpm. The rest of the constants have their usual meaning. This model also includes the impedance behavior of the polymer contacting the inactive electrolyte (absence of the redox couple in solution) by considering $Z_e^{f|s} \rightarrow \infty$ in Eq. (2).

A rigorous fitting procedure was performed employing Eq. (2). Six replicate measurements for each degree of deactivation were carried out, and the error structure was assessed following the method recommended by Agarwal et al. [32] and Orazem [33]. The standard deviation for the real (σ_{Zr}) and imaginary (σ_{Zj}) parts of the impedance followed the form proposed by Orazem (see Eq. (8) of Ref. [33]).

$$\sigma_{Zr} = \sigma_{Zj} = \alpha|Zj| + \beta|Zr| + \gamma|Z|^2 Rm^{-1} + \delta, \qquad (6)$$

where Rm is the current measuring resistor used for the experiment, Zr is the real part of the impedance, and Zj is the imaginary part of the impedance. α, β, γ, and δ are constants that have to be determined. The values of these scaling factors were $\alpha = 0$, $\beta = 4.22 \times 10^{-3} \pm 0.005 \times 10^{-3}$, $\gamma = 2.5 \times 10^{-5} \pm 0.1 \times 10^{-5}$, and $\delta = 4.8 \times 10^{-3} \pm 0.3 \times 10^{-3}$. The error structure was found to follow the same model within the range of the degree of deactivation $0.05 < \theta_c < 0.77$. At θ_c values lower than 0.05, the error structure model parameters had different values, but these results are not reported here. Then, solid lines in Figs. 1, 2, 3 and point representation in Fig. 4 represent the weighted complex nonlinear least squares fit to the data. The regression was weighted by the inverse of the variance of the stochastic part of the measurement. Under all conditions, the weighted sum of the square of residuals was below one [33].

References

1. Barbero C, Silber JJ, Sereno L (1990) Electrochemical properties of poly(*o*-aminophenol) modified electrodes in aqueous acid solutions. J Electroanal Chem 291:81–101
2. Barbero C, Silber JJ, Sereno L (1989) Formation of a novel electroactive film by electropolymerization of *ortho*aminophenol. Study of its chemical structure and formation mechanism. Electropolymerization of analogous compounds. J Electroanal Chem 263:333–352
3. Ohsaka T, Kunimura S, Oyama N (1988) Electrode kinetics of Poly(*o*-aminophenol) film prepared by electrooxidative polymerization of aminophenol and its electrochromic propertes. Electrochim Acta 33:639–645
4. Tucceri RI, Barbero C, Silber JJ, Sereno L, Posadas D (1997) Spectroelectrochemical study of poly(*o*-aminophenol). Electrochim Acta 42:919–927
5. Komura T, Ito Y, Yamaguti T, Takahasi K (1998) Charge-transport processes at poly-*o*-aminophenol film electrodes: electron hopping accompanied by proton exchange. Electrochim Acta 43:723–731
6. Miras MC, Badano A, Bruno MM, Barbero C (2003) Nitric oxide electrochemical sensors based on hybrid films of conducting polymers and metal phtalocyanines. Port Electrochim Acta 21:235–243
7. Yano J, Kawakami H, Yamasaki S, Kanno Y (2001) Cation capture ability and the potential response of a poly(*o*-aminophenol) film electrode to dissolved ferric ions. J Electrochem Soc 148:E61–E65
8. Lobo MJ, Miranda AJ, López-Fonseca JM, Tuñón P (1996) Electrocatalytic detection of nicotinamide coenzymes by poly(*o*-aminophenol) and poly(*o*-phenylenediamine)-modified carbon paste electrode. Anal Chim Acta 325:33–42
9. Zhang AQ, Cui CQ, Lee JY (1996) Metal-polymer interaction in the Ag^+/poly-*o*-aminophenol system. J Electroanal Chem 413:143–151
10. Mu S (2004) Electrochemical copolymerization of aniline and *o*-aminophenol. Synth Met 143:259–268
11. Zhang Y, Mu S, Deng B, Zheng J (2010) Electrochemical removal and release of perchlorate using poly(aniline-co-*o*-aminophenol). J Electroanal Chem 641:1–6
12. Dai J, Tao Y, Gu X, Liu Z, Kong Y, Liu W, Ma J, Wei Y (2015) Electrically controllable perchlorate removal based on poly(aniline-co-*o*-aminophenol) doped with p-toluene sulfonate. J Appl Polym Sci 132:41895
13. Mu S (2006) Catechol sensor using poly(aniline-co-*o*-aminophenol) as an electron transfer mediator. Biosens Bioelectron 21:1237
14. Mu S (2009) Direct determination of arsenate based on its electrocatalytic reduction at the poly(aniline-co-*o*-aminophenol) electrode. Electrochem Commun 11:1519
15. Tucceri R (2014) Effect of prolonged electrode potential cycling on the charge-transport parameters of poly(*o*-aminophenol) films. A study employing rotating disc electrode voltammetry and surface resistance. J Electroanal Chem 717–718:131–139
16. Tucceri R (2005) The effect of high positive potentials on the different charge-transport and charge-transfer parameters of poly(*o*-aminophenol) modified electrodes. A study using cyclic voltammetry, steady-state rotating disc electrode voltammetry and ac impedance measurements. J New Mater Electrochem Syst 8:305–315
17. Tucceri R (2009) Redox mediation and permeation processes at deactivated poly(*o*-aminophenol) films. A study applying rotating disc electrode voltammetry and electrochemical impedance spectroscopy. J Electroanal Chem 633:198–206
18. Tucceri R (2011) Charge-transfer and charge-transport parameters of deactivated poly(*o*-aminophenol) film electrodes. A study employing electrochemical impedance spectroscopy. J Electroanal Chem 659:83–91
19. Tucceri R (2015) Deactivation of poly(*o*-aminophenol) film electrodes by storage without use in the supporting electrolyte solution and its comparison with other deactivation processes. J Electroanal Chem 739:58–65
20. Yang X, Kirsch J, Fergus J, Simonian A (2013) Modeling analysis of electrode fouling during electrolysis of phenolic compounds. Electrochim Acta 94:259–268
21. Vorotyntsev MA, Deslouis C, Musiani MM, Tribollet B, Aoki K (1999) Transport across an electroactive polymer film in contact with media allowing both ionic and electronic interfacial exchange. Electrochim Acta 44:2105–2115
22. Barbero C, Tucceri RI, Posadas D, Silber JJ, Sereno L (1995) Impedance characteristics of poly(*o*-aminophenol) electrodes. Electrochim Acta 40:1037–1040
23. Musiani MM (1990) Characterization of electroactive polymer layers by electrochemical impedance spectroscopy (EIS). Electrochim Acta 35:1665–1670

24. Salavagione HJ, Arias-Padilla J, Pérez JM, Vázquez JL, Morallón E, Miras MC, Barbero C (2005) Study of the redox mechanism of poly(*o*-aminophenol) using in situ techniques: evidence of two redox processes. J Electroanal Chem 576:139–145
25. Levin O, Kondratiev V, Malev V (2005) Charge transfer processes at poly-*o*-phenylenediamine and poly-*o*-aminophenol films. Electrochim Acta 50:1573–1585
26. Bisquert J (2002) Analysis of kinetics of ion intercalation: ion trapping approach to solid-state relaxation processes. Electrochim Acta 47:2435–2449
27. Yano J, Kawakami H, Yamasaki HS (1999) Potential response of a poly(*o*-aminophenol) film electrode to dissolved ferric ions. Synth Met 102:1335
28. Vorotyntsev MA (2002) Impedance of thin films with two mobile charge carriers, interfacial exchange of both species with adjacent media. Effect of the double layer charge. Electrochim Acta 47:2071–2079
29. Vorotyntsev MA, Badiali JP, Inzelt G (1999) Electrochemical impedance spectroscopy of thin films with two mobile charge carriers: effects of the interfacial charging. J Electroanal Chem 472:7–19
30. Vorotyntsev MA, Dikhin LI, Levi MD (1994) Modeling the impedance properties of electrodes coated with electroactive polymer films. J Electroanal Chem 364:37–49
31. Vorotyntsev MA, Badiali JP, Vieil D (1996) Multi-component diffusion approach to transport across electroactive polymer films with two mobile charge carriers. Electrochim Acta 41:1375–1381
32. Agarwal P, Orazem ME, García-Rubio LH (1992) Measurement models for electrochemical impedance spectroscopy. 1. Demonstration of applicability. J Electrochem Soc 139:1917–1927
33. Orazem ME (2004) A systematic approach toward error structure identification for impedance spectroscopy. J Electroanal Chem 572:317–327